AGU PUBLICATIONS

Water Resources Research

RESEARCH ARTICLE
10.1002/2014WR016574

In situ determination of surface relaxivities for unconsolidated sediments

Markus Duschl[1], Petrik Galvosas[2], Timothy I. Brox[2], Andreas Pohlmeier[1], and Harry Vereecken[1]

[1]Agrosphere (IBG-3), Forschungszentrum Jülich GmbH, Jülich, Germany, [2]MacDiarmid Institute for Advanced Materials and Nanotechnology, School of Chemical and Physical Sciences, Victoria University of Wellington, Wellington, New Zealand

Key Points:
- Surface relaxivity serves as calibration parameter for NMR relaxation measurements
- Pore surface measurement method affects the surface relaxivity determination
- NMR diffusion experiments lead to best calibration results

Correspondence to:
P. Galvosas,
petrik.galvosas@vuw.ac.nz

Citation:
Duschl, M., P. Galvosas, T. I. Brox, A. Pohlmeier, and H. Vereecken (2015), In situ determination of surface relaxivities for unconsolidated sediments, *Water Resour. Res.*, *51*, 6549–6563, doi:10.1002/2014WR016574.

Received 22 OCT 2014
Accepted 21 JUL 2015
Accepted article online 24 JUL 2015
Published online 24 AUG 2015

Abstract NMR relaxometry has developed into a method for rapid pore-size determination of natural porous media. Nevertheless, it is prone to uncertainties because of unknown surface relaxivities which depend mainly on the chemical composition of the pore walls as well as on the interfacial dynamics of the pore fluid. The classical approach for the determination of surface relaxivities is the scaling of NMR relaxation times by surface to volume ratios measured by gas adsorption or mercury intrusion. However, it is preferable that a method for the determination of average pore sizes uses the same substance, water, as probe molecule for both relaxometry and surface to volume measurements. One should also ensure that in both experiments the dynamics of the probe molecule takes place on similar length scales, which are in the order of some microns. Therefore, we employed NMR diffusion measurements with different observation times using bipolar pulsed field gradients and applied them to unconsolidated sediments (two purified sands, two natural sands, and one soil). The evaluation by Mitra's short-time model for diffusion in restricted environments yielded information about the surface to volume ratios which is independent of relaxation mechanisms. We point out that methods based on NMR diffusometry yield pore dimensions and surface relaxivities consistent with a pore space as sampled by native pore fluids via the diffusion process. This opens a way to calibrate NMR relaxation measurements with other NMR techniques, providing information about the pore-size distribution of natural porous media directly from relaxometry.

1. Introduction

Prediction of water mobility and retention in soils caused by root water uptake, redistribution, percolation, and runoff generation is of great interest in a range of fields as diverse as agriculture and resources exploration. However, water distribution and flow on a microscopic scale in a complex system like soil is still poorly understood and the pore space structure is a key factor for understanding these water dynamics. In particular in systems with a narrow pore-size distribution, information about the pore surface or pore surface to volume ratio may be sufficient for a first understanding of water distribution and transport. To date, there are various direct and indirect methods available for the characterization of the pore space, such as multistep outflow measurements, gas adsorption isotherms (BET), mercury intrusion, or imaging techniques such as computed tomography [*Brunauer et al*., 1938; *Gliński et al*., 2011; *Petrovic et al*., 1982; *Ritter and Drake*, 1945; *van Dam et al*., 1994]. All these methods have different characteristic length scales on which the pore space is probed and although these methods are well established, they also may be time consuming, expensive, or produce toxic waste.

As an alternative to the techniques described above, nuclear magnetic resonance (NMR) can be used for a quick and nondestructive determination of pore-size distributions and pore surface to volume ratios [*Coates et al*., 1999]. The characteristic length scale of the relevant NMR measurements is defined by the diffusion length of the pore fluid during the sampling period which is typically in the micrometer range. In addition, with NMR it is possible to distinguish between different types of fluids inside the porous medium [*Hedberg et al*., 1993]. Methods for characterization of fluids in porous rocks by NMR were first utilized by the petroleum industry [*Coates et al*., 1999; *Kleinberg et al*., 1994; *Song*, 2012] and later extended to unconsolidated porous media (e.g., soils) [*Jaeger et al*., 2009; *Paetzold et al*., 1985; *Pohlmeier et al*., 2009; *Stallmach et al*., 2002; *Stingaciu et al*., 2010; *Vogt et al*., 2002]. Furthermore, NMR measurements can be applied in the field using portable NMR systems like single-sided low-field NMR devices [*Casanova et al*., 2011].

In conventional NMR relaxometry, the signal amplitude is proportional to the fluid content while the signal decay rates give information about the pore surface to volume ratios and pore wall interactions. However, relaxation rates do not depend solely on the pore surface to volume ratios. Another factor, the surface relaxivity, also influences relaxation rates and it needs to be calibrated if pore-size distributions or pore surface to volume ratios are to be extracted from the NMR relaxometry measurements [*Barrie*, 2000; *Brownstein and Tarr*, 1979; *Howard and Kenyon*, 1992; *Hürlimann et al*., 1994; *Sen et al*., 1994]. Hence, relaxation times which are directly translated into pore-size distributions using only NMR relaxation measurements are prone to systematic errors if the surface relaxivity is unknown. Surface relaxivities depend on the local dynamics of the fluid, on the chemical composition of the solid-fluid interface [*Kleinberg et al*., 1994], and are explicitly linked to NMR measurements. Thus, they cannot be determined directly by non-NMR experiments. A solution is to provide an independent calibration measurement of the pore sizes and to combine it with average NMR relaxation times for the determination of surface relaxivities. There are several experimental methods of characterizing pore sizes: in addition to conventional gas adsorption or mercury intrusion, also NMR methods are available. These methods have the advantage of being sensitive to the same types of dynamics and interactions as the natural pore filling fluid since they use the same probe molecule and time scale as NMR relaxometry.

For the study of flow and diffusion processes, pulsed field gradient nuclear magnetic resonance (PFG NMR) has been in use for a number of decades [*Stejskal and Tanner*, 1965]. In confined systems like porous media, PFG NMR provides information not only about the confined fluid but also about the structure of the porous system [*Callaghan*, 1991]. In particular, the employment of PFG NMR was reported for oilfield exploration and related laboratory experiments to distinguish between mobile and immobile fluid in consolidated sediments [*Fordham et al*., 1994; *Hürlimann et al*., 1994]. However, PFG NMR is not restricted to this field of application as these methods have been used in a pilot study of the pore structure of unconsolidated sediments [*Vogt et al*., 2002]. Further NMR approaches are diffusion tensor methods or double wave vector diffusion-weighting experiments, but also magnetization decay due to diffusion in internal magnetic fields or the combination of NMR relaxation with partial desaturation of the porous media [*Basser et al*., 1994; *Kershaw et al*., 2013; *Koch and Finsterbusch*, 2008; *Mitra*, 1995; *Mohnke*, 2014; *Mutina and Skirda*, 2007; *Song*, 2003].

In natural porous media, susceptibility differences between solid and liquid interfaces as well as paramagnetic impurities lead to internal gradients which interfere with the external magnetic gradients of the diffusion measurements. To overcome these additional effects, a NMR sequence with two pairs of bipolar PFGs was introduced by *Cotts et al*. [1989]. This 13 interval pulse sequence consists of pulsed field gradients of equal amplitudes but opposite polarities in combination with phase inverting 180° rf-pulses so that unknown background gradients do not affect the determination of diffusion coefficients provided the background gradients remain constant during the duration of the experiment. If this condition is not satisfied magic pulsed field gradient (MPFG) NMR as introduced by *Galvosas et al*. [2004] and *Sun et al*. [2003] can be used instead, however, this was not necessary in the present study and the application of the 13 interval pulse sequence was sufficient.

Thus, we present in this study the combination of PFG NMR diffusion measurements and NMR relaxometry on purified and natural sands and a natural soil which differ in pore size and pore-size distribution. This approach is an expansion of the work of *Hürlimann et al*. [1994] for sedimentary rocks. Using both NMR diffusometry and gas adsorption measurements, we have determined the surface to volume (S/V) ratio of these samples and combined both types of S/V measurements with longitudinal and transverse relaxation times to determine surface relaxivities for these unconsolidated sediments. We will point out that NMR diffusion and gas adsorption experiments give different surface to volume ratios depending on their characteristic length scale and the intrinsic fractal nature of porous media [*Daigle et al*., 2014; *Stallmach et al*., 2002]. Finally, we assume that the NMR methods yield pore dimension and surface relaxivity results consistent with a pore space as sampled by native pore fluids if the pore surfaces are not governed by structural details on the nanometer-scale. With the information on surface relaxivities, it is then possible to calibrate NMR relaxation measurements and to obtain information about the pore-size distribution directly from relaxometry [*Hürlimann et al*., 1994].

2. Theory

Nuclear spins within the sample (we observed ^{1}H from the water molecules) in the presence of a static magnetic field B_0 form a macroscopic magnetization while the individual spins precess in equilibrium about the

axis of the B_0 field (which is oriented in the z direction by convention). This macroscopic magnetization is tilted using an additional, orthogonal, and oscillating magnetic field which has a frequency equal to the precession of the nuclear spins and is typically applied as an rf-pulse. After excitation by this pulse, the precessing magnetization can be detected by convenient methods, so-called pulse sequences, along with its relaxation to the equilibrium state. Here, the signal amplitude yields information about the total fluid content within the sample and the relaxation times contain information about the dynamics of the fluid.

In porous media, relaxation times are related to the pore sizes by the fast exchange model of *Brownstein and Tarr* [1979] if one assumes weak pore coupling [*McCall et al*., 1991] and neglects the contribution of diffusion in magnetic field gradients to the transverse relaxation rate,

$$\frac{1}{T_i} = \frac{1}{T_{i,\,\mathrm{bulk}}} + \rho_i \frac{S}{V}\,, \tag{1}$$

with $i = 1$ for longitudinal and $i = 2$ for transverse relaxation. $T_{i,\,\mathrm{bulk}}$ are the relaxation times of bulk water, ρ_i are surface relaxivity parameters, and S/V denotes the pore surface area to pore volume ratio of the porous medium.

The surface relaxivities depend on the surface structure and chemical composition at the solid-fluid interface as well as on the local dynamics of the pore fluid at the interface. Using the Brownstein-Tarr equation (1) it is possible to determine the surface to volume ratio of a saturated porous medium if the surface relaxivity ρ is known and assumed to be homogeneous. With A the specific surface area, ρ_0 the bulk density, and ϕ the porosity of the porous medium, equation (1) can be rewritten as

$$\langle \rho_i \rangle = \left(\frac{1}{\langle T_i \rangle} - \frac{1}{T_{i,\,\mathrm{bulk}}} \right) \frac{\phi}{A \cdot \rho_0}\,, \tag{2}$$

where the brackets $\langle\,\rangle$ indicate average values.

Thus, NMR relaxation measurements can either be used to determine the surface relaxivities if the pore surface to volume ratio is known or vice versa, but it is not possible to gain information about both parameters simultaneously without further knowledge.

It should be noted that a precondition of the Brownstein-Tarr equation (1) is the fast diffusion assumption, which states that the diffusional motion of the water molecules through the entire pore is faster than the surface relaxation. It is controlled by the parameter

$$\kappa_i = \frac{\rho_i r}{2D} \ll 1, \tag{3}$$

with i=1 for longitudinal and i=2 for transverse relaxation, and r describes the characteristic dimension of the pore [*Brownstein and Tarr*, 1979; *Godefroy et al*., 2001]. In porous media, r is assumed to be $r = \eta \cdot \frac{V}{S}$, with the geometric factor η (see below).

In fact, the calculation of the surface relaxivities following equation (1) is only valid if the fast diffusion criterion is applicable, thus $\kappa < 0.1$. In case of a questionable fast diffusion assumption, it is possible to use as a first approximation a more general function between surface relaxivity and relaxation time valid in the intermediate regime [*Godefroy et al*., 2001; *Keating*, 2014]:

$$\rho_2 = \left(\frac{S/V}{T_{2,\mathrm{P}}^{-1} - T_{2,\,\mathrm{bulk}}^{-1}} - \frac{\eta}{2D(S/V)} \right)^{-1}, \tag{4}$$

with $T_{2,\mathrm{P}}^{-1}$ the transverse peak relaxation rate, D the diffusion coefficient and η=2 for cylindrical pores, η=3 for spherical ones, or more general for example η=30 for regular tetrahedral pores where the radius is one-half the length of one side [*Keating and Falzone*, 2013]. Equation (4) has two limiting cases, on the one hand the pure surface limited relaxation process for $\kappa_i \ll 1$, and on the other hand the pure diffusion limited relaxation process with $\kappa_i \gg 1$. In the surface limited case, equation (4) is identical to equation (1) while for the diffusion limited case relaxation processes at the pore walls are assumed to cause instantaneous and complete magnetization loss. In the intermediate regime, the diffusion term in equation (4) acts as a correction term for the surface relaxation due to a reduced mobility of the water molecules in the pores.

Because of the appearance of faster eigenmodes in the relaxation time distribution for measurements when the fast diffusion assumption is not valid, the peak values of the slowest mode of the relaxation time distribution are a good representation of the lowest eigenmodes. Therefore, the peak values may be a more advisable choice for the calculation of the surface relaxivities using equation (4) compared to mean values of the whole relaxation time distribution.

If the fast diffusion assumption is valid, the Bloch-Torrey equation predicts a linear dependence between the relaxation rate and t_E^2, with a slope of $\frac{1}{12}\gamma^2 g^2$ [*Torrey*, 1956]. This is not always the case, in particular for unconsolidated sediments with grain and pore sizes of several tens of micrometers, and the influence of effective internal magnetic field gradients becomes more complex. For a theoretical understanding of the interaction between NMR relaxation and effective field gradients in porous media, one can follow the fundamental works of *Hürlimann* [1998] and *Mitchell et al*. [2010]. Diffusion regimes are defined by the ratios between the dephasing length, the structural length, and the diffusion path length (equations (1)–(6) in *Mitchell et al*. [2010]). The dephasing length l_g is the length scale at which a spin dephases by 2π rad by diffusing within an effective internal gradient g_{eff}

$$l_g = \left(\frac{D_0}{\gamma g_{\text{eff}}}\right)^{1/3}, \tag{5}$$

with D_0 the diffusion coefficient of bulk water and γ the gyromagnetic ratio. As a first approximation, it is possible to obtain the maximum effective gradient without prior knowledge of the pore size and the shape of the magnetic field as [*Mitchell et al*., 2010]

$$g_{\text{eff}} \approx \left(\frac{\gamma}{D_0}\right)^{1/2} (\Delta\chi B_0)^{3/2}, \tag{6}$$

with $\Delta\chi$ the magnetic susceptibility difference at the solid-liquid interface and B_0 the external magnetic field strength. The structural length l_S is a measure for the pore sizes, and the diffusion path length l_E is defined as the length scale a spin diffuses during the echo time t_E

$$l_E \approx \sqrt{D_0 t_E}\,. \tag{7}$$

The different diffusion regimes which are limited by these length scales are (i) the motional averaging regime where both $l_g \gg l_S$ and $l_E \gg l_S$, so usually applicable for small pores, (ii) the localization regime where $l_g \ll l_S$ and $l_E \gg l_S$, so that spins are sensitive to variations in the local magnetic field strength, and (iii) the short-time regime where $l_g \gg l_S$ and $l_E \ll l_S$, so that spins behave as in the case of free diffusion. Note that in the case that two length scales are comparable (i.e., $l_g \approx l_E$, $l_g \approx l_S$, or $l_E \approx l_S$) or in the case that both length scales satisfy $l_g \ll l_S$ and $l_E \ll l_S$, there is no particular diffusion regime defined. As a result, the interactions between relaxation and internal gradients are not well-defined and cannot be analyzed in detail.

In contrast to relaxation measurements, in diffusion experiments there is a direct relationship between the time-dependent apparent self-diffusion coefficient $D_{\text{app}}(t)$ and geometrical properties of the pore space without a surface relaxivity parameter [*Latour et al*., 1993]. In bulk fluid and therefore for unrestricted diffusion, the self-diffusion coefficient is related to the mean square displacement l_0 by

$$l_0^2 = \left[\vec{r}\,(\Delta) - \vec{r}\,(0)\right]^2 = 2nD_0\Delta, \tag{8}$$

where $\vec{r}\,(\Delta)$ is the position at the time Δ, $\vec{r}\,(0)$ is the position at time zero, and D_0 the bulk self-diffusion coefficient. n is related to the dimensionality of the diffusion process and is 1, 2, or 3 for 1-D, 2-D, or 3-D diffusion, respectively. In confined systems, the diffusion path of the water molecules is restricted by the pore walls. Therefore, the apparent self-diffusion coefficient $D_{\text{app}}(\Delta)$ is reduced compared to the self-diffusion coefficient D_0 and it depends on the ratio between the length scale of the confining system and the root mean squared displacement (RMSD) l of the bulk fluid which is determined by the observation time of the diffusion process Δ [*Sen*, 2004]. Due to the interconnectivity of pores, the relationship between the apparent diffusion coefficient and pore geometry can be complicated and may not be accessible based on NMR diffusion measurements alone. However, for short observation times, it was shown by *Mitra et al*. [1992] and

experimentally proven by *Hürlimann et al.* [1994] that the apparent diffusion coefficient decreases with the square root of the observation time Δ following the relation

$$\frac{D_{\mathrm{app}}(\Delta)}{D_0} = 1 - \frac{4}{9\sqrt{\pi}} \frac{S}{V} \sqrt{D_0 \Delta} + \mathcal{O}(D_0 \Delta), \tag{9}$$

where $\mathcal{O}(D_0\Delta)$ describes higher orders of $(D_0\Delta)$. The main term of this "short-time behavior" depends only on the surface to volume ratio S/V and it is independent of any other parameter, in particular independent of the surface chemistry and surface relaxivity.

In the long-time limit as $\Delta \to \infty$, the diffusion coefficient ratio approaches the value $1/\alpha$, with α the tortuosity of the medium which is a measure for the interconnectivity of the pores. Using the short and the long-time behaviors, one can extrapolate and approach the real relation by a two point Padé approximation [*Brown et al.*, 2012; *Mair et al.*, 2001]

$$\frac{D_{\mathrm{app}}(\Delta)}{D_0} = 1 - \left(1 - \frac{1}{\alpha}\right) \left(\frac{\frac{4}{9\sqrt{\pi}} \frac{S}{V} (D_0\Delta)^{1/2} + \left(1 - \frac{1}{\alpha}\right) \frac{D_0 \Delta}{D_0 \theta}}{\left(1 - \frac{1}{\alpha}\right) + \frac{4}{9\sqrt{\pi}} \frac{S}{V} (D_0\Delta)^{1/2} + \left(1 - \frac{1}{\alpha}\right) \frac{D_0 \Delta}{D_0 \theta}} \right), \tag{10}$$

where θ is a fitting parameter in units of time which describes the time a water molecule needs to diffuse the distance of the tortuosity limit.

Common NMR methods for measuring the apparent self-diffusion coefficient are pulsed-field gradient NMR experiments [*Stejskal and Tanner*, 1965; *Tanner*, 1970]. The combination of a NMR diffusion experiment with a NMR relaxation measurement enables both the determination of the pore-size distribution and the surface relaxivities without the need for knowledge about the microscopic pore wall chemistry and NMR relevant interactions at or near the pore wall.

3. Materials and Methods

In this study, four different sand samples and one soil sample were used. For comparison, data from a monodisperse packing (grain diameter of 400 μm) of glass beads (GB) have been reprocessed from literature [*Vogt et al.*, 2002]. Two of the sand samples (SN1 and SN2) were natural quartz sands purchased from Quarzwerke GmbH, Frechen, Germany. The other sand samples (SW1 purchased from Sigma Aldrich Chemie GmbH, Steinheim, Germany, and SW2 purchased from Scientific & Chemical Supplies Ltd., Bilston, UK) were acid washed to remove paramagnetic impurities from the surface of the grains. All sand samples consisted of more than 99% SiO_2 and differed mainly by their grain size and porosity (Table 1). The soil sample (SO) was a sieved ($<$ 2 mm) sandy soil from a test site in Vechtel, Germany which is part of the long-term soil monitoring program of Lower Saxony, Germany. The soil was characterized as a Podzol-Gleysol, horizon A, and contains 95.7% w/w sand, 3.4% w/w silt, and 0.9% w/w clay. The soil information is given according to the current valid "manual of soil mapping" (KA5) of the German Federal Institute for Geosciences and Natural Resources. The fundamental properties of all samples are listed in Table 1. For the determination of the paramagnetic impurities on the surface of the pores, random samples with a mass of 1 g were taken, the impurities were washed off the grains using aqua regia at room temperature, and the solutions were analyzed by ICP-OES. The paramagnetic contents are given as sum of the main parts (compounds of iron and manganese) as mass fractions of the porous media. The given porosity was determined gravimetrically.

For the NMR measurements, all samples were measured fully saturated with deionized water in sample tubes with 13 mm inner diameter and 100 mm height. Centrifugation of the samples at 5000$\times g$ for 5 min before the measurements ensured comparable packing densities and 100% water saturation of the pore space.

High-field NMR diffusion and relaxation experiments on the sand and soil samples were performed at room temperature ($\sim$21°C) using a superconducting vertical wide-bore magnet with a Bruker AVANCE400 spectrometer and a Bruker Micro2.5 microimaging gradient set. The system operated at 400 MHz ^{1}H resonance frequency and contained a 15 mm inner diameter birdcage resonator with a sensitive height of 20 mm. Low-field NMR relaxation measurements were conducted on a home-built Halbach magnet with a ^{1}H resonance frequency of 6.4 MHz [*Raich and Blumler*, 2004]. The low-field system was connected to a STELAR

Table 1. Physical Properties of the Different Samples[a]

Sample	Type	Mean Grain Size (mm)/ Soil Texture (% w/w)	Porosity (-)	Paramagnetic Impurities on the Surface (μg / g_{sample})
GB[b]	Glass beads	0.40	0.35	
SN1	Natural sand	0.35	0.39	26
SN2	Natural sand	0.24	0.43	21
SW1	Acid washed sand	0.22	0.43	13
SW2	Acid washed sand	0.21	0.41	20
SO	Soil	Clay: 0.9, silt: 3.4, sand: 95.7	0.40	1000

[a]The paramagnetic impurities are given as mass fraction of the total sample when washed off the grains of the porous media. Not available information and values are indicated as empty entry.
[b]The properties of the glass beads were determined in *Vogt et al.* [2002].

spectrometer (Stelar, Mede, Italy) and contained a solenoid RF coil with inner diameter of 40 mm and sensitive height of 60 mm.

T_1 relaxation was determined by the inversion recovery (IR) pulse sequence [*Vold et al.*, 1968] which measures the relaxation state of the longitudinal magnetization of the pore fluid as a function of the delay time. This delay time was altered between 2 ms and 20 s in 16 exponentially increasing time steps.

T_2 relaxation was measured by the Carr-Purcell-Meiboom-Gill (CPMG) pulse sequence [*Carr and Purcell*, 1954; *Meiboom and Gill*, 1958], with echo times at high magnetic field ranging from $t_E = 0.2$ ms to $t_E = 5.38$ ms and at low field ranging from $t_E = 0.15$ ms to $t_E = 2$ ms. The repetition time for these experiments was $t_R = 5$ s at both high and low magnetic field strength. The bulk relaxation times of both T_1 and T_2 relaxation were determined by extracting pore water from the samples via centrifugation.

The measurements of the apparent self-diffusion coefficients of water $D_{app}(\Delta)$ in the porous media as a function of the observation time Δ were performed with the 13 interval sequence introduced by *Cotts et al.* [1989] (Figure 1) to suppress disturbances in the NMR signal induced by internal magnetic field gradients [*Kleinberg et al.*, 1994; *Spindler et al.*, 2011; *Stallmach and Galvosas*, 2007]. For a given Δ, the strength of the magnetic field gradients was varied. The gradient pairs were applied in the z direction (vertical), which is the direction of the static magnetic field B_0, and the gradients strength was incremented from 0.01 T/m to the maximum of 1.44 T/m in 32 steps for all samples. In order to attenuate the signal to the noise level with the highest possible gradient strength, the gradient duration δ was set to 1 ms. The observation time Δ was varied from 3.5 ms to 1 s for the sand samples in 21 steps and from 2.58 to 146 ms in 16 steps for the soil sample. The observation time Δ of the soil sample was limited by the shorter longitudinal relaxation time T_1 as compared to the sand samples. All parameters are illustrated in Figure 1.

All acquired data were initially processed with Prospa® (Magritek Ltd., Wellington, New Zealand). Relaxation time distributions were obtained using a home built Matlab-based Inverse Laplace Transformation routine. The relaxation time boundaries were set to a minimum of 100 μs and a maximum of 5 s and calculated for 100 steps. The regularization parameter λ was chosen from the representation of the variance as a function of log λ (L-curve) when λ was varied between 10^7 and 10^{12} in 35 steps. The optimal value for λ as balance between the residual fit error and the influence of the ill-posedness of the inverse problem was chosen at the heel of the L-curve [*Hansen*, 1992; *Song et al.*, 2002].

For the self-diffusion data, $D_{app}(\Delta)$ was obtained from fitting an exponential function to the magnetization decay (M/M_0) normalized on a reference measurement with the same settings with the exception that $g=0$ as function of the gradient strength according to the equation of *Cotts et al.* [1989]

$$\frac{M}{M_0} = \exp\left(-D_{app} \cdot b\right) \tag{11}$$

with $b=(\gamma g \delta)^2 \cdot (4\Delta + 6\tau - 2\delta/3)$, γ the gyromagnetic ratio of hydrogen, g the gradient strength, δ the gradient duration, and τ the spacing between the first two rf pulses. It should be noted that this normalization also suppresses possible effects of surface relaxation during the diffusion measurement. For the final step of data evaluation, the fitting of the two point Padé approximation (equation (10)) to the normalized ratios $D_{app}(\Delta)/D_0$, a Python nonlinear least squares fitting routine was used [*Brown et al.*, 2012].

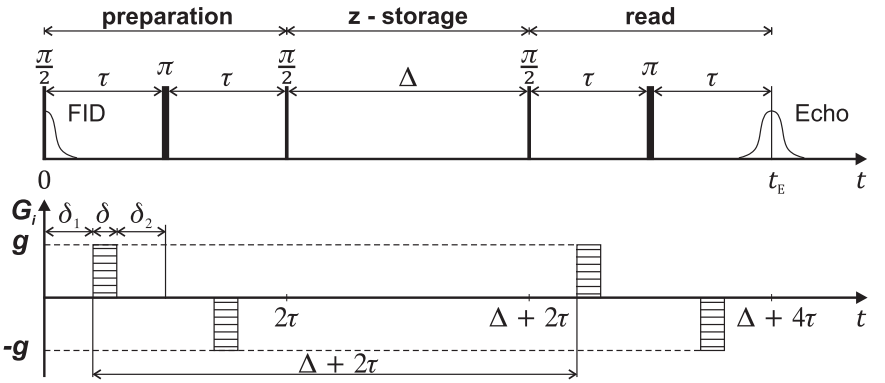

Figure 1. 13 interval pulse sequence with pulsed field gradients G_i with $i=x$, y, or z as introduced by *Cotts et al.* [1989]. The pulse sequence consists of both rf-pulses ($\pi/2$-pulses which rotate the magnetization by 90° and π-pulses with a rotation angle of 180°) (first line) and gradient pulses (second line). The sequence can be divided in three parts, the encoding period when the diffusion measurement is prepared, the evolution period, when the magnetization is stored in the $-z$ direction, and the decoding period when the spin echo containing the information is read. τ describes the time between two rf-pulses during the preparation and read interval while Δ is the observation time which depicts the time the magnetization is stored. The magnetic gradient strengths g are altered during a diffusion experiment and δ is the width of the gradient pulses. Finally, δ_1 and δ_2 describe the time between the rf-pulses and the gradient pulse. The apparent self-diffusion coefficients of water $D_{app}(\Delta)$ were determined as a function of the observation time Δ.

For comparison to a non-NMR method, we measured the specific surface of the porous media with krypton BET. Krypton BET was used instead of standard nitrogen BET because the total surface area of the pore space in the sand samples was too small for nitrogen in our measurement setup. To validate the krypton BET experiments, the soil sample was also measured with nitrogen BET and both techniques yielded the same specific area.

4. Results and Discussion

4.1. Relaxation Experiments

The longitudinal relaxation time distributions at 400 MHz are monomodal except for the soil sample (not shown) so that there is no indication for diffusion-weighting by multimodal pore-size distributions. The resulting mean T_1 times are listed in Table 2. For the glass bead sample and sand samples, all values are higher than 1.5 s which justifies long observation times for the diffusion experiments. The longitudinal relaxation distribution of the soil sample instead shows a bimodal behavior with mean T_1 times of $T_{1,\,fast} = 20$ ms and $T_{1,\,slow} = 110$ ms which limits the longest possible observation time to $\Delta = 146$ ms.

The effective T_2 distributions obtained with a CPMG-sequence reveal bimodal shapes for all sands and a broader range of T_2 times for the soil sample for both magnetic field strengths (400 MHz, Figure 2a, and 6.4 MHz, Figure 2b). The slow modes contribute at least 90% to the total areas for the sand samples while for the soil all modes are approximately equal. It should be noted that if the fast diffusion limit cannot be assumed

Table 2. Mean Longitudinal and Transverse Relaxation Times of the Glass Beads (GB), Quartz Sands (SN1, SN2, SW1, SW2), and Soil (SO) Samples[a]

		$T_{2,M}^{eff}$ (s)		$T_{2,P}^{eff}$ (s)	
Sample	$T_{1,M}$ (s) at 400 MHz	At 400 MHz	At 6.4 MHz	At 400 MHz	At 6.4 MHz
GB[b]	2.08	0.169			
SN1	2.35 ± 0.04	0.33 ± 0.02	0.67 ± 0.03	0.40	0.69
SN2	1.54 ± 0.05	0.22 ± 0.01	0.55 ± 0.02	0.26	0.59
SW1	1.54 ± 0.04	0.25 ± 0.01	0.59 ± 0.02	0.29	0.65
SW2	1.60 ± 0.04	0.13 ± 0.01	0.25 ± 0.01	0.15	0.25
SO	0.06 ± 0.01	0.017 ± 0.002	0.19 ± 0.04		

[a]The transverse relaxation times are given for an echo time of $t_E = 0.2$ ms at 400 MHz and an echo time of $t_E = 0.3$ ms at 6.4 MHz. The $T_{1,M}$ times are given as weighted arithmetic means of the relaxation time distributions, while the T_2 times appear both as mean relaxation times $T_{2,M}^{eff}$ and as peak relaxation times of the slowest relaxation mode $T_{2,P}^{eff}$. The transverse relaxation times are noted as "effective" T_2^{eff} because they are not corrected for the influence of internal gradients.
[b]Adopted from *Vogt et al.* [2002].

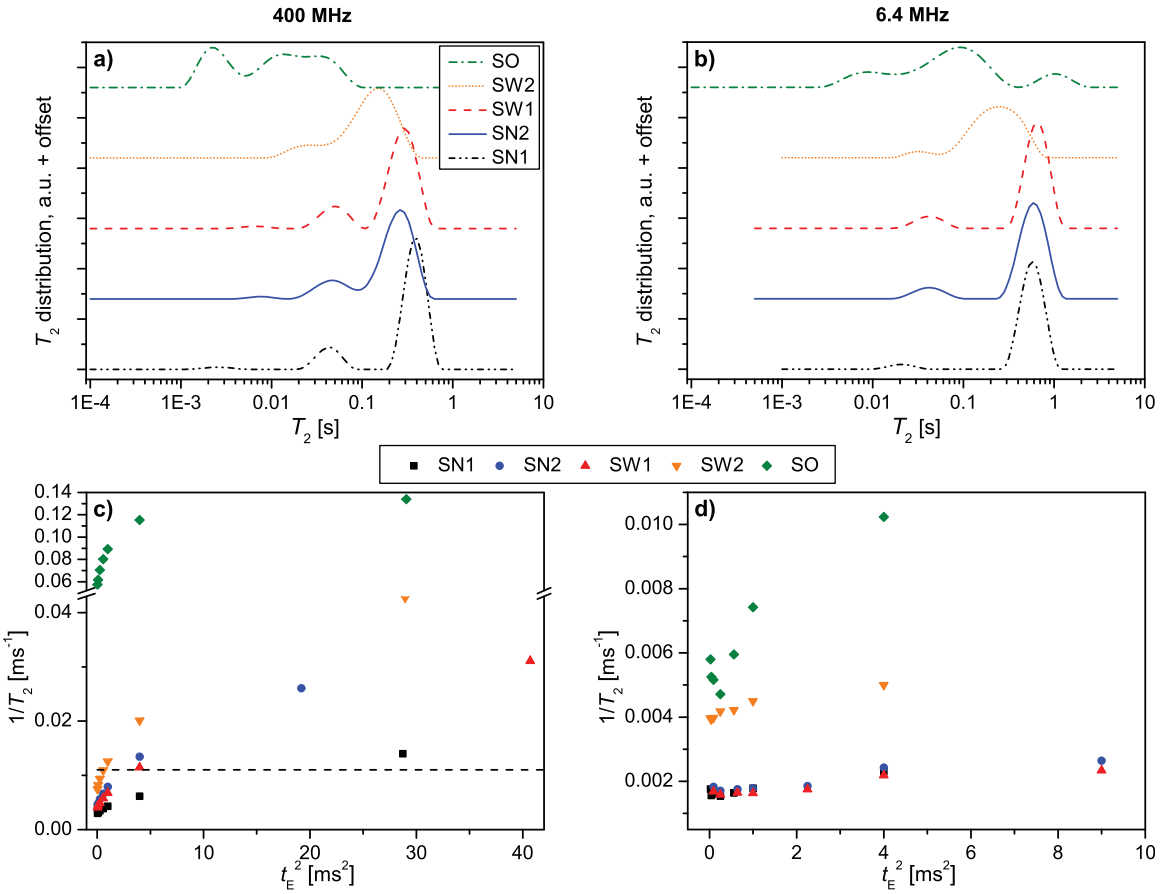

Figure 2. (a) Effective transverse relaxation time distributions at 400 MHz ($t_E = 0.2$ ms) and (b) at 6.4 MHz ($t_E = 0.3$ ms) obtained by inverse Laplace transformation of the CPMG data. The notations refer to the samples as described in Table 1. (c) Echo time dependence of the mean transverse relaxation rates as a function of t_E^2 in high magnetic field and (d) in low field. Note the different scale in Figure 2d as compared to Figure 2c as indicated by the dotted line in Figure 2c.

to be true, the resulting relaxation time distribution shows not only contributions of different pore environments but also higher eigenmodes of the relaxation process.[*Godefroy et al.*, 2001; *Keating*, 2014; *Mohnke and Klitzsch*, 2010; *Ryu and Johnson*, 2009]. In this case, the peak relaxation times of the slowest modes, $T_{2,P}^{eff}$, may be a more appropriate representation than the weighted arithmetic means $T_{2,M}^{eff}$ because $T_{2,P}^{eff}$ then would represent the slowest eigenmode [*Dlugosch et al.*, 2013]. Therefore, both values are given in Table 2.

The influence of diffusion within internal magnetic field gradients was determined by echo-time dependent CPMG measurements and by the comparison of low and high magnetic field strengths. The shift in the mean transverse relaxation time by approximately a factor of two for the sand samples between 6.4 MHz and 400 MHz demonstrates the influence of the magnetic field strength via internal field gradients caused by susceptibility differences [*Washburn et al.*, 2008] (Figures 2a and 2b). The arithmetic means of the T_2 relaxation times as a function of the echo time are shown in Figure 2c for high field and in Figure 2d for low field. It is clear that for the shortest echo time of $t_E = 0.2$ ms no significant influence of t_E on the transverse relaxation time has to be taken into account.

Figures 2c and 2d further show that the linear dependence between the relaxation rate and t_E^2, as predicted from the Bloch-Torrey equation is not met [*Torrey*, 1956]. For a more detailed analysis of the effect of internal gradients on the relaxation data, we followed the work of *Mitchell et al.* [2010] (equations (5)–(7)). We can estimate the internal gradients (equation (5)) with $\Delta\chi_{app}$, the apparent volumetric magnetic susceptibility difference at the solid-liquid interface of quartz sand $\left(\Delta\chi_{app} \approx 10^{-5}\right)$ (adopted from *Mullins* [1977]). For our sand samples, it yields maximum gradients as large as 0.6 T/m at 6.4 MHz, and 300 T/m at 400 MHz. The dephasing length l_g is then approximately 2.4 μm in the low field and 0.3 μm for the high field, while the structural length l_S is about 70 μm for the example of the SN2 sample, and the diffusion path length l_E is about 0.7 μm during the echo period of $t_E = 0.2$ ms. Hence, both $l_g \ll l_S$ and $l_E \ll l_S$, and $l_g \approx l_E$, so that our measurements are not performed in any of

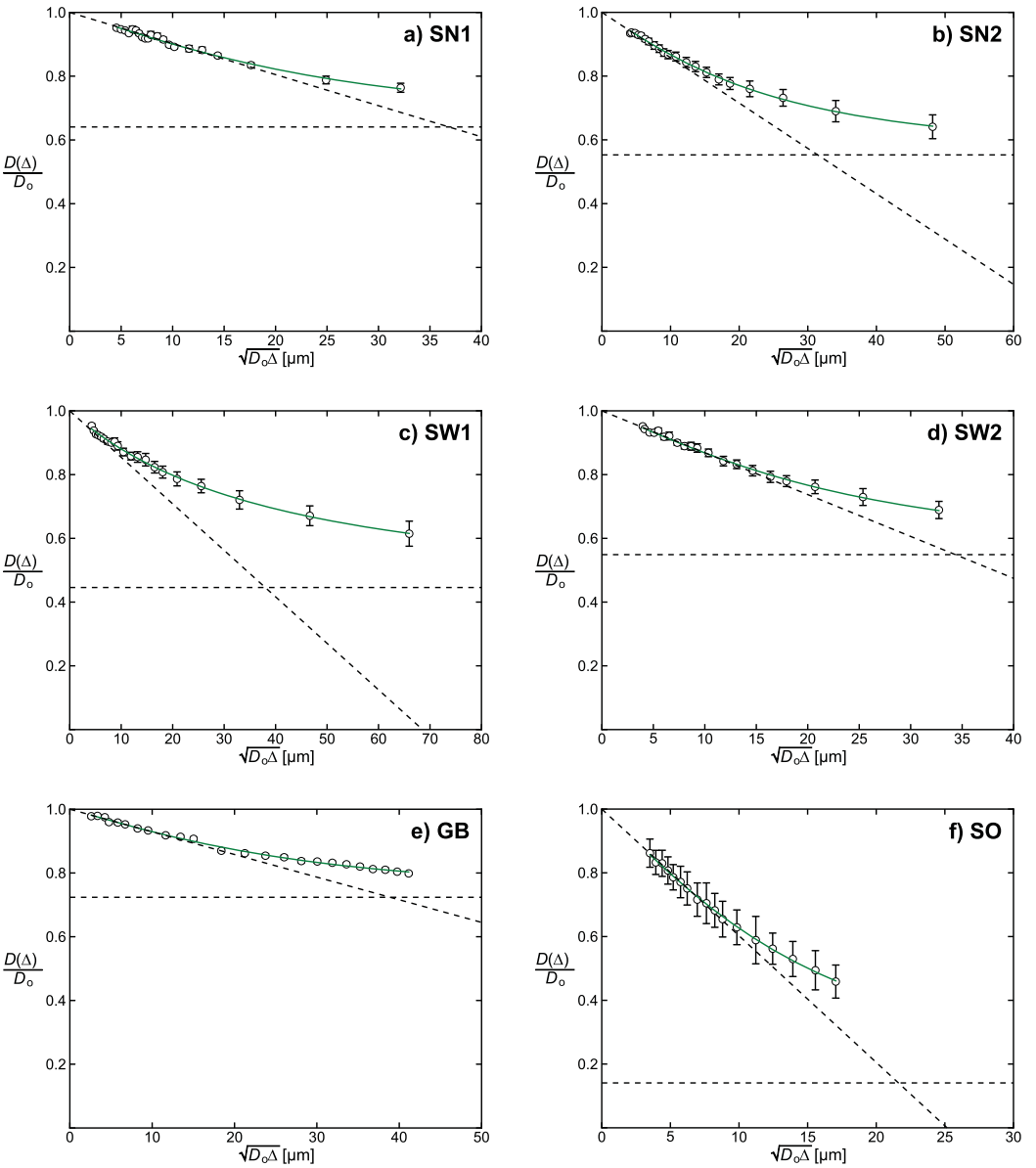

Figure 3. Relative apparent self-diffusion coefficients $D(\Delta)/D_0$ as function of the square root of the observation time $\sqrt{\Delta}$ of the natural sand samples SN1 (a) and SN2 (b), the acid-washed sand samples SW1 (c) and SW2 (d), of the glass bead sample (e) (reprocessed from *Vogt et al.* [2002]), and of the soil sample SO (f). The solid lines show the fits of the Padé approximation. The horizontal-dashed lines represent the long-time limits while the sloped dashed lines represent the initial slopes of the short-time behavior, from which the surface to volume ratios are obtained.

the specified diffusion regimes where the echo time dependence of the magnetic decay would be well-defined but halfway between the short-time and the localization regime. Hence, the measured mean relaxation times should be termed as effective times $T_{2,\,\mathrm{eff}}$ which imply both contributions of true T_2 relaxation and effects of diffusion in internal gradients. Nevertheless, the existence of a dependence of the NMR signal amplitude on t_E shows that internal gradients occur, and the diffusion measurements should be performed with bipolar pulsed field gradient pairs to compensate for such effects [*Cotts et al.*, 1989].

4.2. Diffusion Measurements and Surface to Volume Ratios

Apparent self-diffusion coefficients of water were determined as a function of the observation times. The fitted two point Padé approximations (equation (10)) to the normalized ratios $D_{\mathrm{app}}(\Delta)/D_0$ as a function of $\sqrt{D_0\Delta}$ are shown in Figure 3 where the data of the glass beads were adopted from *Vogt et al.* [2002] and reprocessed.

Table 3. Fitted Bulk Diffusion Coefficients and Surface to Volume Ratios From Diffusion Experiments, BET Measurements, and a Model Calculation[a]

		S/V (μm^{-1})		
Sample	D_0 (10^{-9} m^2/s)	Diffusion (S/V_{NMR})	BET (S/V_{BET})	Model[b] (S/V_{Model})
GB[c]	2.26 ± 0.03	0.028 ± 0.005		0.028
SN1	2.07 ± 0.03	0.039 ± 0.005	0.29 ± 0.01	0.027
SN2	2.32 ± 0.03	0.057 ± 0.005	0.29 ± 0.01	0.033
SW1	2.18 ± 0.03	0.058 ± 0.005	0.18 ± 0.01	0.036
SW2	2.15 ± 0.03	0.052 ± 0.005	0.11 ± 0.01	0.041
SO	1.93 ± 0.03	0.159 ± 0.008	(Kr BET) 0.89 ± 0.01 (N_2 BET) 0.87 ± 0.01	

[a]The notations refer to the samples as described in Table 1.
[b]The reference surface to volume ratio is calculated by a model (equation (12)). There is no error given for the modelled values because the determination of the model error is beyond the scope of this study.
[c]The properties of the glass beads are adopted from *Vogt et al.* [2002] and recalculated. There was no BET measurement performed for the glass beads.

The initial slopes of these approximations (Figure 3) depend on the surface to volume ratios only. They are represented by the sloped-dashed lines, whereas the horizontal-dashed lines show the limit of the diffusion coefficient for long times and represent the inverse tortuosity $1/\alpha$. Although the uncertainty of $1/\alpha$ is comparably high due to limited maximum observation times Δ, this does not affect the determination of S/V which is contained in the initial slope. Furthermore, the correctness of the procedure is validated since all apparent diffusion coefficients are smaller than the bulk diffusion coefficient D_0.

The resulting fitting parameters D_0 and S/V are included in Table 3. Also included are surface to volume ratios measured with krypton BET and, for comparison, the calculation of S/V by a geometrical model,

$$\frac{S}{V} = 6\left(\frac{1}{\phi} - 1\right)\frac{1}{d_g}, \tag{12}$$

where the surface to volume ratio of a random packing of spherical grains is estimated from the grain diameter d_g and porosity ϕ [*Latour et al.*, 1993]. The model is based upon the assumption that the packing consists of a homogeneous distribution of grains of the same size which approach a spherical shape. Therefore, it is not appropriate to apply this model to the soil sample with a broad grain-size distribution.

The diffusion measurement of the soil sample was more challenging than the quartz sand measurements because of the fast relaxation rates. In fact, the contribution of the fast mode to the T_2 relaxation time distribution counts for relaxation times shorter than 5 ms and therefore it does not contribute to the diffusion signal because the smallest possible period τ between the first two RF pulses was τ = 5.4 ms. It is noteworthy that soil samples with a higher amount of silt and clay, resulting in smaller pores, typically have relaxation times in this range or even shorter so that the decay of the magnetization is too fast for diffusion experiments performed with this pulse sequence.

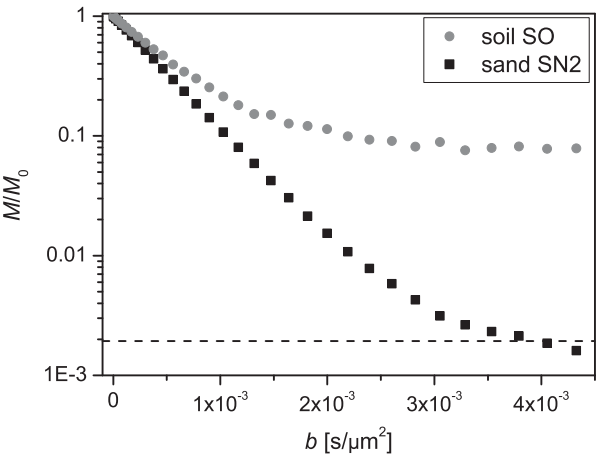

Figure 4. Example of the relative magnetization decay M/M_0 as a function of b for one observation time (Δ = 3.5 ms) for the soil sample SO (dots) and one quartz sand sample SN2 (squares). The dashed line represents the noise level.

One example of the relative magnetization decay depending on the gradient strength for the soil sample (dots) is shown in Figure 4 together with the comparative result for the SN2 sample (squares). The dashed line represents the noise level. One can see that the magnetization of the soil sample reaches an offset of about 10% of the total magnetization at high gradient strengths instead of reaching the noise level, as observed in the

Table 4. Longitudinal and Transverse Surface Relaxivities Calculated by Equation (1) Using Effective Relaxation Times and S/V Ratios from Diffusion Measurements, BET Surface Determination, and a Model Calculation[a]

	ρ_1 (μm/s)			ρ_2 (μm/s) at 400 MHz			ρ_2 (μm/s) at 6.4 MHz		
Sample	Diffusion	BET	Model[b]	Diffusion	BET	Model[b]	Diffusion	BET	Model[b]
GB[c]	5.3		5.3	196		194			
SN1	2.4 ± 0.5	0.3 ± 0.1	3.4	60 ± 20	8 ± 1	91	25 ± 6	3.3 ± 0.3	36
SN2	5.6 ± 0.5	1.1 ± 0.1	9.7	70 ± 10	14 ± 1	124	26 ± 4	5.0 ± 0.3	45
SW1	5.5 ± 0.5	1.7 ± 0.3	8.8	60 ± 10	20 ± 2	98	21 ± 4	6.7 ± 0.5	34
SW2	5.6 ± 0.6	2.7 ± 0.7	7.2	130 ± 20	60 ± 10	171	70 ± 10	31 ± 5	85
SO	90 ± 20	17 ± 3		360 ± 50	65 ± 8		32 ± 3	5.7 ± 0.7	

[a]The notations of the samples are described in Table 1.
[b]The used model of a random packing of spherical grains is described in equation (12).
[c]The properties of the glass beads are adopted from *Vogt et al*. [2002] and recalculated.

sand. This is due to small pore fractions in the soil sample containing water which is practically immobile [*Jäger et al*., 2011; *Jaynes et al*., 1995], but which leads to the bimodal longitudinal relaxation time distribution as discussed in the relaxation experiments section. This indicates a weighting of the diffusion measurement towards the slow mode in particular for long observation times. Thus, the apparent self-diffusion coefficients $D_{app}(\Delta)$ were determined for small gradient strengths only using the initial slope of the magnetization decay. The result is included in Figure 3f. Due to the offset shown in Figure 4 and the resulting smaller number of data points available for the determination of the diffusion coefficients, the relative errors of the apparent diffusion coefficients are higher for the soil than for the sand samples (Figure 3f).

The most striking point concerning surface to volume ratios is that the BET measurements yield greater values than the NMR diffusion experiments by a factor of 2–6 (Table 3). We can explain this by the different surface morphologies to which the two methods are sensitive. On the one hand, during NMR measurements the water molecules diffuse through a surface layer of water averaging over structures smaller than the dephasing length of about 0.3 to 2.4 μm, and water molecules trapped in small confinements do not contribute to the signal due to the fast relaxation [*Stallmach et al*., 2002]. On the other hand, BET is measuring adsorption and desorption using gas isotherms so that the surface averaging takes place on the scale of the size of the probe gas atom or molecule which is usually some orders of magnitude smaller than the dephasing length in NMR experiments. Despite the differences between S/V_{NMR} and S/V_{BET}, both are generally in good agreement with corresponding values reported in literature. *Grunewald and Knight* [2011] published $S/V_{BET}=0.53\ \mu m^{-1}$ for a quartz sand with a mean grain diameter between 0.12 mm and 0.21 mm (for comparison see Table 1) and *Vogt et al*. [2002] reported S/V_{NMR} between $0.023\ \mu m^{-1}$ and $0.045\ \mu m^{-1}$ for different quartz sands at 400 MHz. The reported surface to volume ratios are typically higher for rock samples than for unconsolidated sediments due to the different pore structure, but the S/V_{NMR} and S/V_{BET} differ as much or even more than the values reported here. For instance, *Hürlimann et al*. [1994] published S/V_{NMR} between $0.023\ \mu m^{-1}$ and $0.48\ \mu m^{-1}$ for a series of different rock samples at 85 MHz while the S/V_{BET} of the same samples was reported as $0.48\ \mu m^{-1}$ up to $1.7\ \mu m^{-1}$. However, *Fleury* [2007] reported for a series of SiC grain packs S/V_{NMR} measurements between $0.17\ \mu m^{-1}$ and $1.3\ \mu m^{-1}$ at 2 MHz and stated that the surface explored by NMR and by BET technique are the same.

For comparison, the geometric model (equation (12)) estimates the surface to volume ratio of a packing of spherical grains. It agrees closest with the experimental data of the spherical glass beads but with respect to S/V of the sands, the model fits the NMR data better than the BET results. Thus, we have demonstrated that for NMR measurements, the averaging effect of the probe molecules leads to a closer agreement between the experimental results and the spherical model and for sands it is a reasonable estimate of the surface to volume ratio [*Vogt et al*., 2002].

4.3. Surface Relaxivities

The longitudinal and effective transverse surface relaxivities ρ_1 and ρ_2 calculated via equation (1) using S/V_{NMR}, S/V_{Model}, or S/V_{BET} and the mean relaxation times are summarized in Table 4. It should be noted that these are effective values since they are calculated from the effective mean transverse relaxation times which imply contributions from true T_2 and from diffusion in internal gradients. The bulk relaxation times used for the calculation of the surface relaxivities were determined as $T_{1,\,bulk}$ to range from 2.8 to 2.9 s and

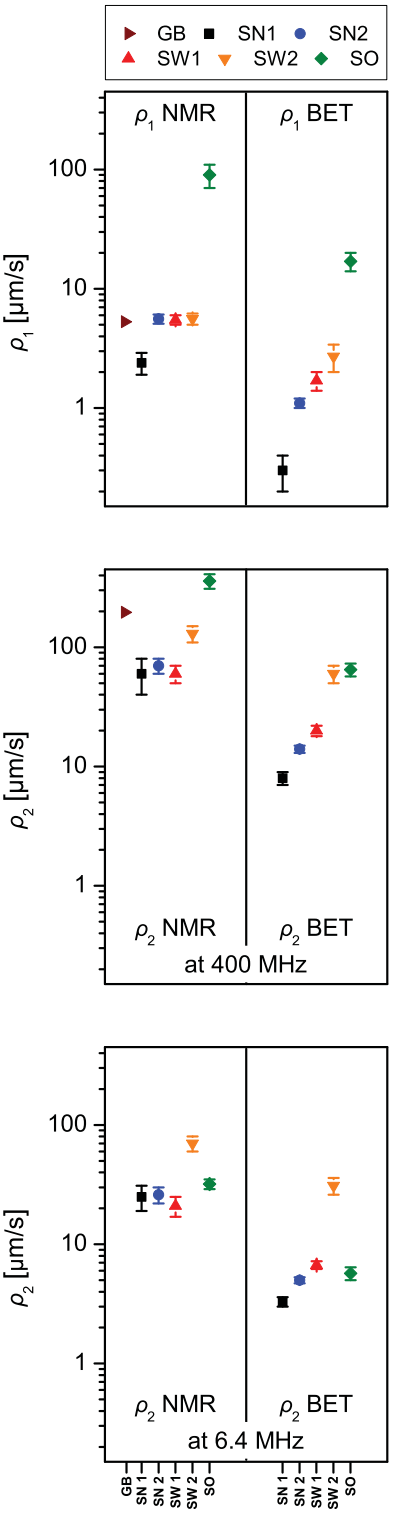

Figure 5. Longitudinal and transverse surface relaxivities of all samples for the different measurement methods. Notations are set according to Table 1. Note that the surface relaxivities are plotted versus arbitrary sample numbers. The surface relaxivities are calculated from the surface to volume ratios in combination with the mean relaxation times (see Table 4). "$\rho_{1,2}$ NMR" and "$\rho_{1,2}$ BET" refer to the calculation using either S/V_{NMR} or S/V_{BET} (Table 3) and the respective effective relaxation times (Table 2).

as $T_{2,\,bulk}$ to range from 1.8 to 2.1 s for all samples. The differences in the surface to volume ratios directly translate to the differences in the surface relaxivities. The longitudinal surface relaxivities of the glass bead and sand samples, obtained from S/V_{NMR}, range from 2 to 6 μm/s and are in good agreement with literature data [*Hürlimann et al.*, 1994]. Based upon the NMR diffusion measurements, ρ_1 of the soil sample is 90 μm/s, where the increased surface relaxivity is due to enhanced relaxation rates caused by the higher content of paramagnetic impurities (see Table 1).

Due to faster transverse relaxation, the transverse surface relaxivities at 400 MHz range from 60 to 360 μm/s and are about one order of magnitude higher than ρ_1 for the sand samples and a factor of four higher for the soil sample. At 6.4 MHz, compared to the high field values, ρ_2 is reduced by a factor of two for the sand samples and a factor of 10 for the soil sample due to the slower effective relaxation rates. Thus, the transverse surface relaxivities may be prone to the influence of internal gradients [*Mitchell et al.*, 2010]. Additionally, transverse relaxation rates and ρ_2 are dependent on the external magnetic field strength.

The surface relaxivity values resulting from the model calculations are in the same range as the NMR values due to similar surface to volume ratios, while calculations based on the BET measurements differ by a factor of 2–6. The higher estimates of the surface relaxivity in the BET calculations reflect the higher surface to volume ratios measured with this technique.

To visualize the surface relaxivity trends, the data from Table 4 are displayed graphically in Figure 5. It is noteworthy that for each sample ρ_1 is always smaller than ρ_2, for a given magnetic field strength and independent of the pore surface measurement, which agrees with the theory. Additionally, for the sand samples both the ρ_1 NMR and the ρ_2 NMR (calculated using S/V_{NMR}) do not show a trend accounting for the same surface material of these samples. In contrast, clear trends are observed in the surface relaxivity data calculated using BET measurements and these follow the inverse trend in the BET surface to volume ratios (right hand sides).

The NMR surface relaxivities are comparable to values in the literature where the longitudinal surface relaxivity vary between 5 and 20 μm/s in sandstones, sand, and soil materials [*Hürlimann et al.*, 1994; *Pohlmeier et al.*, 2009]. For the transverse surface relaxivities, the reported values for pure SiO_2 sand deduced from S/V_{BET} of 0.5 μm/s at 2.2 MHz fit to the trend of our results at higher magnetic field strengths [*Grunewald and Knight*, 2011]. Also, *Fleury*

Table 5. Comparison of Surface Relaxivities Calculated Using Equation (4) Valid in the Intermediate Regime for the Quartz Sand Samples[a]

	$\rho_{2,\mathrm{cyl}}$ (μm/s) at 400 MHz		$\rho_{2,\mathrm{sph}}$ (μm/s) at 400 MHz	
Sample	Diffusion	BET	Diffusion	BET
SN1	137	6.8	897	6.8
SN2	106	11.6	176	11.7
SW1	83	16.7	124	17.1
SW2	−3347[b]	73	−211[b]	87

[a] $\rho_{2,\mathrm{cyl}}$ were calculated using $\eta=2$ while $\rho_{2,\mathrm{sph}}$ were determined with $\eta=3$ for spherical pores. Both NMR and BET measurements were used for the pore surface to volume ratios.

[b] Negative surface relaxivities are not reasonable and indicate the limitations of the method.

[2007] reported ρ_2 between 1.2 and 3 μm/s for SiC grain packs at 2 MHz. These values are smaller than those we have determined in this work for some natural sands. However, S/V of the SiC samples were considerably higher, surface chemistry is different, and B_0 was smaller which makes a direct comparison difficult. Since effective T_2 and therefore ρ_2 are considerably affected by the background field strength B_0 and via field strength dependent internal gradients [*Korb and Bryant*, 2001; *Mitchell et al*., 2010], the values determined here are indeed comparable.

Nevertheless, as discussed before, our measurements were not performed in a defined diffusion regime. In particular, the fast diffusion assumption may not be met for all experiments. Therefore, equation (4) may be a more appropriate choice to calculate the surface relaxivities. Assuming the pore geometry in first approximation is cylindrical ($\eta=2$) or spherical ($\eta=3$), the resulting surface relaxivities of the quartz sand samples at high magnetic field strength are listed in Table 5 for both NMR and BET pore surface to volume ratios. In particular the ρ_2 using S/V_{NMR} show a significant dependence on the pore geometry while this dependence for ρ_2 using S/V_{BET} is less pronounced because of the much higher surface to volume ratios. This is another indication of measurements which do not meet the fast diffusion criterion. Although the real pore geometry is unknown, quartz sand pores are certainly neither cylindrical nor spherical but are irregularly shaped. Additionally, indicators for a fractal nature of the pore surface of quartz sand have been reported [*Stallmach et al*., 2002] and would suggest much higher values for the geometry factor, such as $\eta=30$ proposed by *Keating and Falzone* [2013]. Nevertheless, a drawback of equation (4) is its dependence of the surface relaxivity on the unknown pore geometry and therefore the need for pore surface measurements which are assumed to reflect more realistic pore geometries.

Another problem of this method is the possibility that negative values may appear for the surface relaxivities (see ρ_2 NMR for the SW2 sample in Table 5). This happens if the second term in equation (4), which describes relaxation by diffusion in the pore fluid, dominates the whole relaxation process. In this case, it is impossible to determine a reasonable surface relaxivity from the NMR relaxation data.

In conclusion, the surface relaxivities shown in Table 4 represent a lower limit, in particular for ρ_2, because no correction of diffusion effects in bulk fluid, which depends on the pore geometry, is used. With respect to the effective pore size, one has to recall that the surface relaxivities depend on the scaling with either S/V_{BET} or S/V_{NMR}. S/V_{NMR} yields self-consistent values for the lower limit of the surface relaxivities of the sands leading to a narrow clustering of the surface relaxivities for samples with similar pore surface chemistry, a result not observed in calculations using BET (see Figure 5). This indicates that NMR diffusion measurements are more suitable to scale NMR relaxation time distributions into pore-size distributions than BET experiments since the former probe pore space on comparable length scales.

5. Conclusions

NMR measurements of the apparent diffusion coefficient, as a function of observation time, were used to determine the surface to volume ratios of the pore space in quartz sand and soil samples. The values determined with NMR (0.039–0.159 $\mu\mathrm{m}^{-1}$) are approximately one order of magnitude smaller than values derived from BET measurements (0.29–0.88 $\mu\mathrm{m}^{-1}$). While both the NMR and BET estimates of S/V agree with values published in the literature, surface to volume ratios from model calculations of the glass bead and sand samples, assuming a random packing of spherical grains, generally agree with the NMR-based estimates. Finally, surface to volume ratios were used in combination with NMR relaxation experiments to determine surface relaxivities. Once known, these surface relaxivities act as a calibration allowing NMR relaxation measurements alone to be used as a fast characterization of the pore space provided the same magnetic field strength is used for both measurements.

Comparing the different methods for estimating surface to volume ratios, we propose that NMR diffusion measurements are more suitable to calculate the surface relaxivities than BET measurements. Due to the fractal nature of the surface of natural porous media [*Stallmach et al.*, 2002], the S/V_{NMR} is more appropriate as it uses water as probing molecule and is measured on the same timescale as the relaxation NMR experiments. As a result, the NMR approach is preferable for the determination of effective pore sizes.

In addition, NMR works with the natural pore fluid moving in the pore space, so it probes the pore grain interface in a way which might be more relevant for hydrological processes than other methods which are performed with pore filling fluids other than water. Hence, regarding flow, fluid transport, or fluid mobilization in porous media, we believe that NMR diffusion measurements yield more suitable pore space information.

Acknowledgments
The data for this paper are available upon request from the authors. This work was supported by CROP.SENSe.net: Networking Sensor Technology Research and Development for Crop Breeding and Management (BMBF 0315529) and by the Royal Society of New Zealand (Marsden Fund). The authors thank M. Fleury (IFP Energies Nouvelles, France) for helpful discussions, C. Walraf and F.-H. Haegel (IBG-3, Forschungszentrum Jülich GmbH, Germany) for the BET measurements as well as Dr. S. Giertz (Department of Geography, University of Bonn, Germany) for the laser diffraction analysis of the SW2 sample.

References

Barrie, P. J. (2000), Characterization of porous media using NMR methods, *Annu. Rep. NMR Spectrosc.*, *41*, 265–316.
Basser, P. J., J. Mattiello, and D. LeBihan (1994), MR diffusion tensor spectroscopy and imaging, *Biophys. J.*, *66*(1), 259–267.
Brown, J. R., T. I. Brox, S. J. Vogt, J. D. Seymour, M. L. Skidmore, and S. L. Codd (2012), Magnetic resonance diffusion and relaxation characterization of water in the unfrozen vein network in polycrystalline ice and its response to microbial metabolic products, *J. Magn. Reson.*, *225*, 17–24.
Brownstein, K. R., and C. E. Tarr (1979), Importance of classical diffusion in NMR-studies of water in biological cells, *Phys. Rev. A*, *19*(6), 2446–2453.
Brunauer, S., P. H. Emmett, and E. Teller (1938), Adsorption of gases in multimolecular layers, *J. Am. Chem. Soc.*, *60*(2), 309–319.
Callaghan, P. T. (1991), *Principles of Nuclear Magnetic Resonance Microscopy*, Oxford Univ. Press, Oxford, U. K.
Carr, H. Y., and E. M. Purcell (1954), Effects of diffusion on free precession in nuclear magnetic resonance experiments, *Phys. Rev.*, *94*(3), 630–638.
Casanova, F., J. Perlo, and B. Blümich (2011), *Single-Sided NMR*, Springer, Berlin.
Coates, G. R., L. Xiao, and M. G. Prammer (1999), *NMR Logging: Principles and Applications*, 251 pp., Halliburton Energy Serv., Houston, Tex.
Cotts, R. M., M. J. R. Hoch, T. Sun, and J. T. Markert (1989), Pulsed field gradient stimulated echo methods for improved NMR diffusion measurements in heterogeneous systems, *J. Magn. Reson.*, *83*(2), 252–266.
Daigle, H., A. Johnson, and B. Thomas (2014), Determining fractal dimension from nuclear magnetic resonance data in rocks with internal magnetic field gradients, *Geophysics*, *79*(6), D425–D431.
Dlugosch, R., T. Gunther, M. Muller-Petke, and U. Yaramanci (2013), Improved prediction of hydraulic conductivity for coarse-grained, unconsolidated material from nuclear magnetic resonance, *Geophysics*, *78*(4), En55–En64.
Fleury, M. (2007), NMR surface relaxivity determination using NMR apparent diffusion curves and BET measurements, paper presented at International Symposium of the Society of Core Analysts, Soc. of Core Anal., Calgary, Canada, 10–12 Sept.
Fordham, E. J., S. J. Gibbs, and L. D. Hall (1994), Partially restricted diffusion in a permeable sandstone: Observations by stimulated echo PFG NMR, *Magn. Reson. Imaging*, *12*(2), 279–284.
Galvosas, P., F. Stallmach, and J. Karger (2004), Background gradient suppression in stimulated echo NMR diffusion studies using magic pulsed field gradient ratios, *J. Magn. Reson.*, *166*(2), 164–173.
Gliński, J., J. Horabik, and J. Lipiec (2011), *Encyclopedia of Agrophysics*, 900 pp., Springer, Dordrecht, Netherlands.
Godefroy, S., J. P. Korb, M. Fleury, and R. G. Bryant (2001), Surface nuclear magnetic relaxation and dynamics of water and oil in macroporous media, *Phys. Rev. E*, *64*(2 Pt 1), 021605.
Grunewald, E., and R. Knight (2011), A laboratory study of NMR relaxation times in unconsolidated heterogeneous sediments, *Geophysics*, *76*(4), G73–G83.
Hansen, P. C. (1992), Analysis of discrete Ill-posed problems by means of the L-curve, *SIAM Rev.*, *34*(4), 561–580.
Hedberg, S. A., R. J. Knight, A. L. Mackay, and K. P. Whittall (1993), The use of nuclear-magnetic-resonance for studying and detecting hydrocarbon contaminants in porous rocks, *Water Resour. Res.*, *29*(4), 1163–1170.
Howard, J. J., and W. E. Kenyon (1992), Determination of pore size distribution in sedimentary rocks by proton nuclear magnetic resonance, *Mar. Petrol. Geol.*, *9*(2), 139–145.
Hürlimann, M. D. (1998), Effective gradients in porous media due to susceptibility differences, *J. Magn. Reson.*, *131*(2), 232–240.
Hürlimann, M. D., K. G. Helmer, L. L. Latour, and C. H. Sotak (1994), Restricted diffusion in sedimentary-rocks: Determination of surface-area-to-volume ratio and surface relaxivity, *J. Magn. Reson. Ser. A*, *111*(2), 169–178.
Jaeger, F., S. Bowe, H. Van As, and G. E. Schaumann (2009), Evaluation of ^{1}H NMR relaxometry for the assessment of pore-size distribution in soil samples, *Eur. J. Soil Sci.*, *60*(6), 1052–1064.
Jäger, A., G. E. Schaumann, and M. Bertmer (2011), Optimized NMR spectroscopic strategy to characterize water dynamics in soil samples, *Organ. Geochem.*, *42*(8), 917–925.
Jaynes, D. B., S. D. Logsdon, and R. Horton (1995), Field method for measuring mobile immobile water-content and solute transfer rate coefficient, *Soil Sci. Soc. Am. J.*, *59*(2), 352–356.
Keating, K. (2014), A laboratory study to determine the effect of surface area and bead diameter on NMR relaxation rates of glass bead packs, *Near Surf. Geophys.*, *12*(2), 243–254.
Keating, K., and S. Falzone (2013), Relating nuclear magnetic resonance relaxation time distributions to void-size distributions for unconsolidated sand packs, *Geophysics*, *78*(6), D461–D472.
Kershaw, J., C. Leuze, I. Aoki, T. Obata, I. Kanno, H. Ito, Y. Yamaguchi, and H. Handa (2013), Systematic changes to the apparent diffusion tensor of in vivo rat brain measured with an oscillating-gradient spin-echo sequence, *NeuroImage*, *70*, 10–20.
Kleinberg, R. L., W. E. Kenyon, and P. P. Mitra (1994), Mechanism of NMR relaxation of fluids in rock, *J. Magn. Reson. Ser. A*, *108*(2), 206–214.
Koch, M. A., and J. Finsterbusch (2008), Compartment size estimation with double wave vector diffusion-weighted imaging, *Magn. Reson. Med.*, *60*(1), 90–101.
Korb, J. P., and R. G. Bryant (2001), The physical basis for the magnetic field dependence of proton spin-lattice relaxation rates in proteins, *J. Chem. Phys.*, *115*(23), 10,964–10,974.

Latour, L. L., P. P. Mitra, R. L. Kleinberg, and C. H. Sotak (1993), Time-dependent diffusion-coefficient of fluids in porous-media as a probe of surface-to-volume ratio, *J. Magn. Reson. Ser. A*, *101*(3), 342–346.
Mair, R. W., M. D. Hurlimann, P. N. Sen, L. M. Schwartz, S. Patz, and R. L. Walsworth (2001), Tortuosity measurement and the effects of finite pulse widths on xenon gas diffusion NMR studies of porous media, *Magn. Reson. Imaging*, *19*(3–4), 345–351.
McCall, K. R., D. L. Johnson, and R. A. Guyer (1991), Magnetization evolution in connected pore systems, *Physical Rev. B*, *44*(14), 7344–7355.
Meiboom, S., and D. Gill (1958), Modified spin-echo method for measuring nuclear relaxation times, *Rev. Sci. Instrum.*, *29*(8), 688–691.
Mitchell, J., T. C. Chandrasekera, and L. F. Gladden (2010), Obtaining true transverse relaxation time distributions in high-field NMR measurements of saturated porous media: Removing the influence of internal gradients, *J. Chem. Phys.*, *132*(24), 244705.
Mitra, P. P. (1995), Multiple wave-vector extensions of the NMR pulsed-field-gradient spin-echo diffusion measurement, *Phys. Rev. B*, *51*(21), 15,074–15,078.
Mitra, P. P., P. N. Sen, L. M. Schwartz, and P. Ledoussal (1992), Diffusion propagator as a probe of the structure of porous-media, *Phys. Rev. Lett.*, *68*(24), 3555–3558.
Mohnke, O. (2014), Jointly deriving NMR surface relaxivity and pore size distributions by NMR relaxation experiments on partially desaturated rocks, *Water Resour. Res.*, *50*, 5309–5321, doi:10.1002/2014WR015282.
Mohnke, O., and N. Klitzsch (2010), Microscale simulations of NMR relaxation in porous media considering internal field gradients, *Vadose Zone J.*, *9*(4), 846–857.
Mullins, C. E. (1977), Magnetic susceptibility of the soil and its significance in soil science: A review, *J. Soil Sci.*, *28*(2), 223–246.
Mutina, A. R., and V. D. Skirda (2007), Porous media characterization by PFG and IMFG NMR, *J. Magn. Reson.*, *188*(1), 122–128.
Paetzold, R. F., G. A. Matzkanin, and A. De Los Santos (1985), Surface soil water content measurement using pulsed nuclear magnetic resonance techniques, *Soil Sci. Soc. Am. J.*, *49*(3), 537–540.
Petrovic, A. M., J. E. Siebert, and P. E. Rieke (1982), Soil bulk density analysis in three dimensions by computed tomographic scanning, *Soil Sci. Soc. Am. J.*, *46*(3), 445–450.
Pohlmeier, A., S. Haber-Pohlmeier, and S. Stapf (2009), A fast field cycling nuclear magnetic resonance relaxometry study of natural soils, *Vadose Zone J.*, *8*(3), 735–742.
Raich, H., and P. Blumler (2004), Design and construction of a dipolar Halbach array with a homogeneous field from identical bar magnets: NMR Mandhalas, *Concept Magn. Reson. B*, *23B*(1), 16–25.
Ritter, H. L., and L. C. Drake (1945), Pore-size distribution in porous materials .1. Pressure porosimeter and determination of complete macropore-size distributions, *Ind. Eng. Chem. Anal. Ed.*, *17*(12), 782–786.
Ryu, S., and D. L. Johnson (2009), Aspects of diffusive-relaxation dynamics with a nonuniform, partially absorbing boundary in general porous media, *Phys. Rev. Lett.*, *103*(11), 118701.
Sen, P. N. (2004), Time-dependent diffusion coefficient as a probe of geometry, *Concept Magn. Reson. A*, *23A*(1), 1–21.
Sen, P. N., L. M. Schwartz, and P. P. Mitra (1994), Probing the structure of porous media using NMR spin echoes, *Magn. Reson. Imaging*, *12*(2), 227–230.
Song, Y. Q. (2003), Using internal magnetic fields to obtain pore size distributions of porous media, *Concept Magn. Reson.*, *18A*(2), 97–110.
Song, Y. Q. (2012), Focus on the physics of magnetic resonance on porous media, *New J. Phys.*, *14*(5), 055017.
Song, Y. Q., L. Venkataramanan, M. D. Hurlimann, M. Flaum, P. Frulla, and C. Straley (2002), T(1)–T(2) correlation spectra obtained using a fast two-dimensional Laplace inversion, *J. Magn. Reson.*, *154*(2), 261–268.
Spindler, N., P. Galvosas, A. Pohlmeier, and H. Vereecken (2011), NMR velocimetry with 13-interval stimulated echo multi-slice imaging in natural porous media under low flow rates, *J. Magn. Reson.*, *212*(1), 216–223.
Stallmach, F., and P. Galvosas (2007), Spin echo NMR diffusion studies, *Annu. Rep. NMR Spectrosc.*, *61*, 51–131.
Stallmach, F., C. Vogt, J. Karger, K. Helbig, and F. Jacobs (2002), Fractal geometry of surface areas of sand grains probed by pulsed field gradient NMR, *Phys. Rev. Lett.*, *88*(10), 105505.
Stejskal, E. O., and J. E. Tanner (1965), Spin diffusion measurements: Spin echoes in the presence of a time-dependent field gradient, *J. Chem. Phys.*, *42*(1), 288.
Stingaciu, L. R., L. Weihermüller, S. Haber-Pohlmeier, S. Stapf, H. Vereecken, and A. Pohlmeier (2010), Determination of pore size distribution and hydraulic properties using nuclear magnetic resonance relaxometry: A comparative study of laboratory methods, *Water Resour. Res.*, *46*, W11510, doi:10.1029/2009WR008686.
Sun, P. Z., J. G. Seland, and D. Cory (2003), Background gradient suppression in pulsed gradient stimulated echo measurements, *J. Magn. Reson.*, *161*(2), 168–173.
Tanner, J. E. (1970), Use of stimulated echo in NMR-diffusion studies, *J. Chem. Phys.*, *52*(5), 2523.
Torrey, H. C. (1956), Bloch equations with diffusion terms, *Phys. Rev.*, *104*(3), 563–565.
van Dam, J. C., J. N. M. Stricker, and P. Droogers (1994), Inverse method to determine soil hydraulic functions from multistep outflow experiments, *Soil Sci. Soc. Am. J.*, *58*(3), 647–652.
Vogt, C., P. Galvosas, N. Klitzsch, and F. Stallmach (2002), Self-diffusion studies of pore fluids in unconsolidated sediments by PFG NMR, *J. Appl. Geophys.*, *50*(4), 455–467.
Vold, R. L., J. S. Waugh, M. P. Klein, and D. E. Phelps (1968), Measurement of spin relaxation in complex systems, *J. Chem. Phys.*, *48*(8), 3831.
Washburn, K. E., C. D. Eccles, and P. T. Callaghan (2008), The dependence on magnetic field strength of correlated internal gradient relaxation time distributions in heterogeneous materials, *J. Magn. Reson.*, *194*(1), 33–40.